City, University of London Institutional Repository

Ultimate tensile behavior of bolted stiffened T-stub connections in progressive collapse resistance

Ying Zhang[1], Shan Gao[2*,3], Lanhui Guo[2], Feng Fu[4], Sheliang Wang[1]

1. School of Civil Engineering, Xi'an University of Architecture and Technology, Xi'an 710055, China

2. School of Civil Engineering, Harbin Institute of Technology, Harbin 150090, China

3. Postdoctoral Station of Civil Engineering, Chongqing University, Chongqing, China

4. School of Mathematics, Computer Science & Engineering, City, University of London, London, EC1V0HB, UK

Abstract: This paper investigates the ultimate tensile behavior of the bolted stiffened T-stub connections using experimental, numerical, and analytical methods. The monotonic tensile tests were carried out on sixteen bolted stiffened T-stub connections with different parameters to investigate the failure mode, yield line distribution, and key mechanical properties of them. The results showed that the distribution pattern of the yield line along the center of the bolt holes changed with the increase of the stiffened T-stub thickness and the longitudinal bolt pitch. The effect of the longitudinal bolt pitch on the ultimate strength of the connection was non-monotonic. Finite element models of the bolted stiffened T-stub connections were established and validated to conduct the parametric analysis. The simulation results showed that increasing the thickness ratio between the vertical plate and the horizontal plate could improve the ultimate strength of the connection. Based on the experimental and parametric studies, the prediction methods for the ultimate strength and initial stiffness of the stiffened T-stub connections with or without bolt pretension were proposed and validated against the experimental data and other prediction methods.

Keywords: Bolted stiffened connection; Bolt pretension; Tensile behavior; T-stub; Progressive collapse; Component method

1. Introduction

Bolted endplate connections are typical semi-rigid connections in the standards for anti-collapse design [1-2]. The advantages of good deformation ability and easy construction make this type of connection be widely studied and recommended in the anti-collapse design by many researchers [3-5]. However, the existing research shows that compared with other semi-rigid connections, the stiffness, and energy dissipation capacity

of bolted end-plate connections are relatively lower [6]. Therefore, a stiffened extended endplate would be better to improve the mechanical behavior of the connection, as shown in Fig. 1.

In the component method in EC3 [7] which is normally used to analyze and predict the mechanical behavior of bolted steel connections, T-stub is treated as the basic component in assembling the bolted connections as shown in Fig. 1. However, bolted stiffened T-stub is not covered by EC3. Therefore it is necessary to conduct an experimental study on the ultimate tensile behavior of bolted stiffened T-stub and develop the corresponding theoretical method for the stiffened connection for practical application.
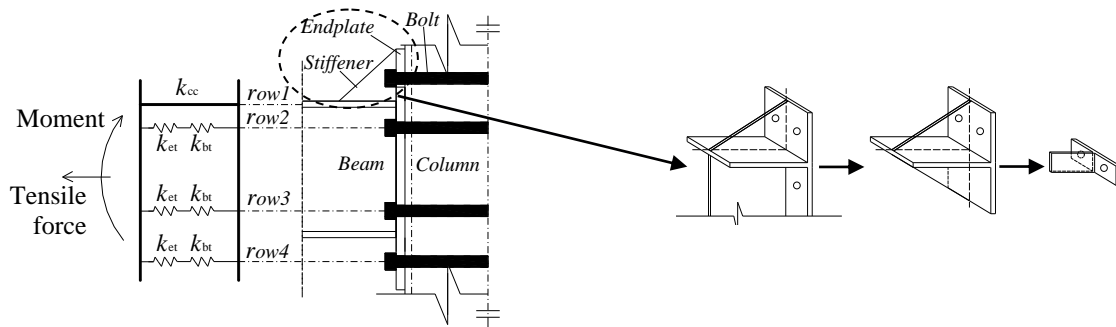

Fig. 1 T-stub in the component method

At present, the research on bolted T-stub connections mainly focuses on unstiffened T-stub connections. Aiming at the flexural behavior of the T-stub, Loureiro et al. [8] and Reinosa et al. [9,10] studied the bending performance of bolted T-stubs and proposed the axial and rotational stiffness prediction formulas. Zhao [11] proposed the numerical models for the force-deformation response of the connections. The determination method of initial yield point and limit state point was more accurate than Jaspart's model [12]. Saberi et al. [13] concluded that the endplate thickness was negatively correlated with the moment ultimate strength. Tagawa and Liu [14] presented a new stiffening method for bolted endplate beam-column connections and the accuracy of the formula was verified by the tensile test of T-stub connection. Ozkilic [15] proposed a new yield line pattern and ultimate load calculation formula for T-stubs with thin plates and large bolts. Gil et al. [16] predicted the stiffness and strength of the T-stub connection under bending by using the method of parameter analysis. The anti-seismic of the bolted T-stub connections has also been studied recently. Shen and Astaneh-Asl [17,18], and Malaga-Chuquitaype and Elghazouli [19] carried out experimental studies and theoretical analyses on the hysteretic performance of the connection respectively. The established models were in good agreement with the experimental results. Ribeiro et al. [20] proposed an analysis method for the T-stub under impact load, which accurately described the force-displacement response of the T-stub model under static and dynamic load.

2

In the design of anti-collapse resistance, a lot of studies have been made on the tensile performance of the bolted T-stub connection by using experimental, numerical and analytical methods. Massimoetal et al. [21], Faralli et al. [22], Francavilla et al. [23], Bursi and Jaspart [24] and Sebbagh et al. [25] used finite element models to analyze the mechanical behavior of T-stub connection in progressive collapse resistance. Yang and Tan [26], and Gong [27] carried out experimental studies and theoretical analyses on the deformation response and ultimate tensile performance of bolted connections. Timmers [28] proposed a model that could accurately reproduce the failure mode and ultimate load of T-stubs. Bezerra et al. [29] studied the plastic deformation capacity of stainless steel bolted T-stub connections. In addition, Barata et al. [30], Gao et al. [31], Wang et al. [32] and Both et al. [33] studied the effects of environment and high temperature on the fire resistance, ultimate tensile performance and failure mode of T-stub connection through experimental and numerical analysis.

It can be seen from the literature review that most of the existing studies have studied the flexural behavior, anti-seismic and anti-collapse of the unstiffened T-stub connections. However, there is limited research on the mechanical performance of stiffened T-stub connections. Therefore, more tests should be conducted to provide experimental evidence to validate various numerical and theoretical studies for bolted stiffened T-stub connections. In this paper, an experimental study on sixteen bolted stiffened T-stub connections was conducted. The tensile performance of the bolted stiffened T-stub connections including the ultimate strength, initial stiffness and deformation capacities were evaluated in terms of various connection design parameters. The validated finite element models for the connections were adopted to conduct parametric analysis. In addition, the prediction methods for the ultimate strength and initial stiffness of the connection were also proposed.

2. Test program

2.1. Test specimens

In total sixteen T-stub specimens were fabricated and tested in this study. To study the influence of bolt pretension, each group consisted of two identical stiffened T-stubs as shown in Table 1. The dimensions of the T-stubs are summarized in Fig. 2 and Table 1. g_H and g_L stand for the horizontal and longitudinal bolt pitch respectively. The stiffeners were installed in the middle of the T-stub.

Grade 8.8 M20 bolts were used for all the specimens except for the last group TSS7 with Grade 8.8 M24 bolts. The diameter of the bolt hole was 2 mm larger than that of the screws. According to Chinese standard JGJ82-2011, the bolt pretension for Grade 8.8 M20 and M24 bolts was 125 kN and 175 kN respectively. The

pretension was converted into torque and applied to the connection through a torque wrench. The installation torque was derived by multiplying the pretension, bolt diameter and torque-pretension coefficient which was 0.15. The specimens without bolt pretension were manually tightened. Washers were used to increase the contact area and prevent the bolts from loosening. In the design of the connection, the prying force in the connection had been checked by using American LFRD manual. The T-stub thickness of the connections all met the requirements of the LFRD.

The specimens were named by group number, followed by P or NP (meaning with or without bolt pretension respectively) and design parameters. Group TSS0 was the standard group. Group TSS1 to group TSS7 referred to four design parameters including stiffened T-stub thickness t, horizontal bolt pitch g_H, longitudinal bolt pitch g_L and bolt diameter d respectively.

The specimens were tested under a monotonic tensile force. Firstly, the stiffened T-stub and the loading device were assembled, and then the vertical plate of the stiffened T-stub and the loading base were clamped on the loading heads of the testing machine respectively as shown in Fig. 2. The displacement control loading method with a speed of 0.025mm/s was used in the experiment.

Table 1 Parameters of specimens								
Specimen No.	L_V [mm]	L_H [mm]	L_L [mm]	t [mm]	g_H [mm]	g_L [mm]	d [mm]	pretension [kN]
TSS0-P	240	190	160	10	50	40	20	125
TSS0-NP	240	190	160	10	50	40	20	0
TSS1-P-t8	240	190	160	**8**	50	40	20	125
TSS1-NP-t8	240	190	160	**8**	50	40	20	0
TSS2-P-t12	240	190	160	**12**	50	40	20	125
TSS2-NP-t12	240	190	160	**12**	50	40	20	0
TSS3-P-H70	260	290	160	10	**70**	40	20	125
TSS3-NP-H70	260	290	160	10	**70**	40	20	0
TSS4-P-H90	260	290	160	10	**90**	40	20	125
TSS4-NP-H90	260	290	160	10	**90**	40	20	0
TSS5-P-L50	240	190	180	10	50	**50**	20	125
TSS5-NP-L50	240	190	180	10	50	**50**	20	0

TSS6-P-L60	240	190	200	10	50	**60**	20	125
TSS6-NP-L60	240	190	200	10	50	**60**	20	0
TSS7-P-d24	240	190	160	10	50	40	**24**	**175**
TSS7-NP-d24	240	190	160	10	50	40	**24**	**0**

Note: L_V is the length of the vertical plate; L_H is the length of the horizontal leg; L_L is the length of the stiffened T-stub; g_H is the length of the horizontal bolt pitch; g_L is the length of the longitudinal bolt pitch; t is the stiffened T-stub thickness; d is the bolt diameter.

Front view   Left view   Top view   Bottom clamping head
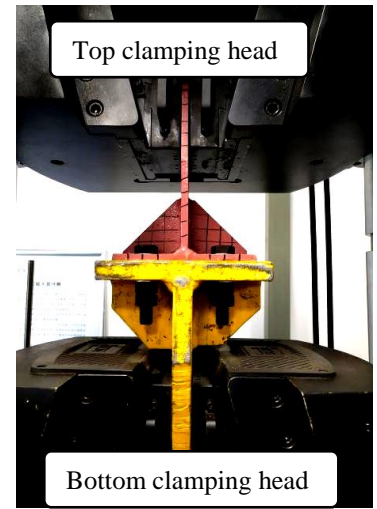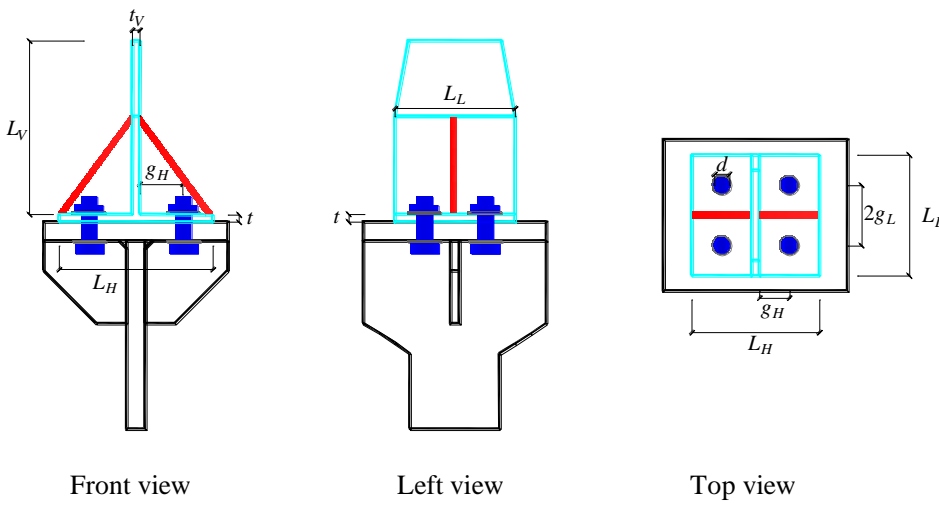
Design of specimens   Test setup

Fig. 2 Design of specimens and test setup

2.2. Mechanical properties of steel

Stiffened T-stub and loading device were both made of Chinese Q235 grade steel. The yield strength f_y, ultimate strength f_u, Young's modulus E_s and ultimate strain ε_u of the steel were given in Table 2. The mechanical properties of the bolts were provided by the supplier. According to the ultimate strain ε_u obtained from the material property test, the true strain $\varepsilon_{u\text{-}true}$ of the tensile specimen can be calculated by Eq. (1) as listed in Table 2.

$$\varepsilon_{u-true} = \ln(1 + \varepsilon_u) \tag{1}$$

Table 2 Material property of steel						
Specimens	Thickness(diameter) [mm]	F_y [MPa]	F_u [MPa]	E_s [MPa]	ε_u	$\varepsilon_{u\text{-}true}$
T-stub	8	232	379	1.78×10^5	0.27	0.24
	10	216	434	1.99×10^5	0.27	0.24

	12	297	420	1.82×10^5	0.28	0.25
M20	20	628	811	2.34×10^5	0.09	0.09
M24	24	633	864	2.34×10^5	0.09	0.09

3. Experimental results

3.1. Failure modes

Three failure modes were observed in the sixteen bolted stiffened T-stub connections under monotonic tensile action, as shown in Figs. 3-5. The first failure mode was the yield of stiffened T-stub and bolts, as shown in Fig. 3. This failure mode was observed in most specimens, including TSS0, TSS3, TSS4, TSS7, TSS2-NP-t12, and TSS5-P-L50. Under the action of monotone tensile load, the horizontal leg of stiffened T-stub deformed first. When the load increased, the deformation of the horizontal leg expanded from heel to end. The deformation extended to the bolt hole and the bolts began to deform. When the stiffened T-stub and bolt reached the yield limit, the bolted stiffened T-stub connection failed.

The second failure mode was found in the specimens TSS2-P-t12 and TSS5-NP-L50, that is, bolt fracture with yielded stiffened T-stub, as shown in Fig. 4. Similarly, the stiffened T-stub began to deform first and started at the heel. The main deformation region was from the heel of the horizontal leg to the bolt hole centerline, and the yield line was distributed along the heel and the deformation direction of the horizontal leg. In this failure mode, the bolt fractured earlier than the stiffened T-stub. It is because when the deformation extended to the centerline of the bolt hole, the bolts began to deform and reached the yield limit earlier than the stiffened T-stub. As the load continued to increase, the bolt fractured first.

The last failure mode was observed in TSS1 and TSS6, that is, stiffened T-stub fracture near bolt hole line and weld seam. It should be noted that the fracture mentioned here does not refer to the weld fracture itself, but the fracture of the metal plate near the weld. The main reason for this failure mode is that the stiffness ratio of stiffened T-stub and bolt was less than 1. When the deformation of stiffened T-stub appeared near the bolt hole, the deformation of the horizontal leg from heel to the centerline of bolt hole continued to increase with the increase of load. As the bolt stiffness was greater than that of stiffened T-stub, the stiffened T-stub fractured first. The yield lines were distributed along with the fracture location and the deformation direction of the horizontal leg.
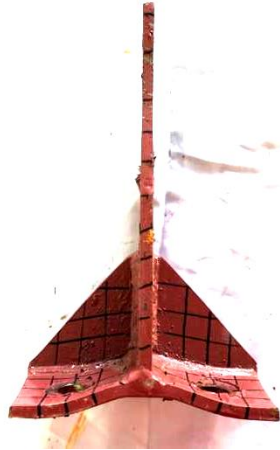
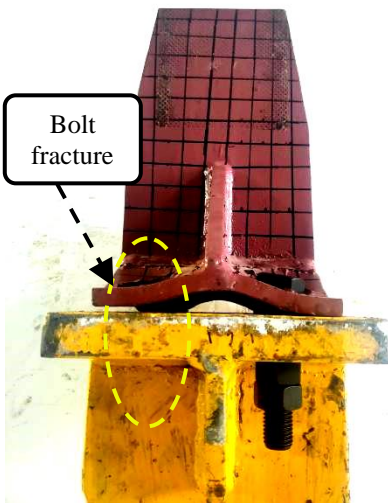|		
(a) Final failure after unloading	(b) Stiffened T-stub yielded	(c) Bolts yielded

Fig. 3 Stiffened T-stub and bolt both yielded (TSS0, TSS3, TSS4, TSS7, TSS2-NP-t12, TSS5-P-L50)
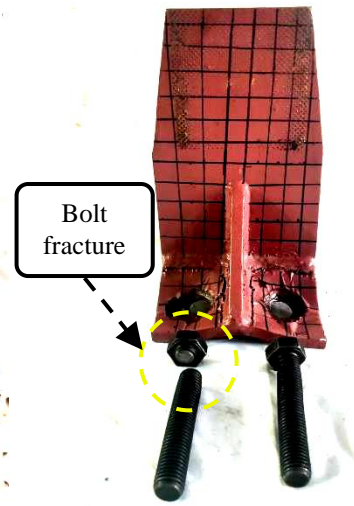
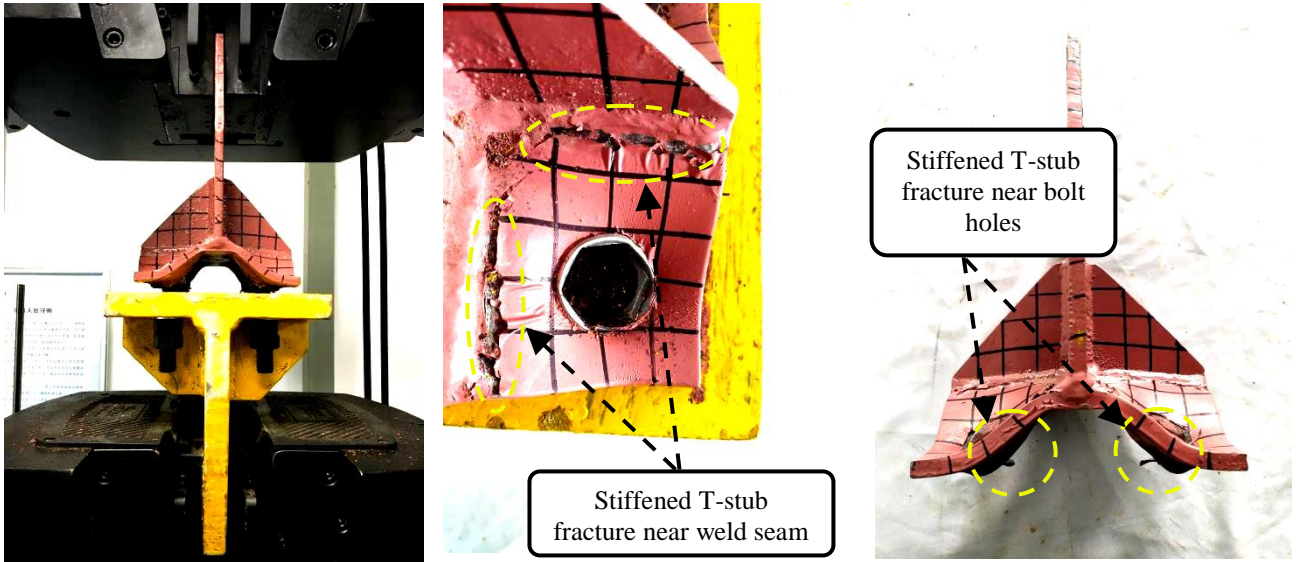|		
(a) Final failure after unloading	(b) Stiffened T-stub yielded	(c) Bolt fracture

Fig. 4 Bolt fracture with yielded stiffened T-stub (TSS2-P-t12, TSS5-NP-L50)

(a) Final failure after unloading

(b) Stiffened T-stub fracture near weld seam

(c) Stiffened T-stub fracture near bolt holes

Fig. 5 Stiffened T-stub fracture near bolt hole line and weld seam (TSS1, TSS6)

The failure modes and main test results of each specimen are summarized in Table 3. Among them, the ultimate deformation given in Table 3 refers to the deformation corresponding to the ultimate load of the specimen. The initial stiffness was calculated by using two points A (D_1,L_1) and B (D_2,L_2) from the elastic stage of the load-displacement curve, taking namely $k=(L_2-L_1)/(D_2-D_1)$.

Specimen No.	Ultimate load [kN]	Ultimate displacement [mm]	Initial stiffness [kN/mm]	Failure mode
TSS0-P	585	47	50	Stiffened T-stub and bolt both yielded
TSS0-NP	575	49	38	Stiffened T-stub and bolt both yielded
TSS1-P-t8	506	37	39	Stiffened T-stub fracture at bolt hole line and weld seam
TSS1-NP-t8	532	41	36	Stiffened T-stub fracture at bolt hole line and weld seam
TSS2-P-t12	692	33	55	Bolt fracture with yielded stiffened T-stub
TSS2-NP-t12	605	49	45	Stiffened T-stub and bolt both yielded
TSS3-P-H70	584	44	42	Stiffened T-stub and bolt both yielded
TSS3-NP-H70	578	70	18	Stiffened T-stub and bolt both yielded
TSS4-P-H90	584	61	33	Stiffened T-stub and bolt both yielded
TSS4-NP-H90	589	65	21	Stiffened T-stub and bolt both yielded

Table 3 Failure patterns

TSS5-P-L50	579	41	33	Stiffened T-stub and bolt both yielded
TSS5-NP-L50	588	45	31	Bolt fracture with yielded stiffened T-stub
TSS6-P-L60	585	47	28	Stiffened T-stub fracture at bolt hole line and weld seam
TSS6-NP-L60	575	49	18	Stiffened T-stub fracture at bolt hole line and weld seam
TSS7-P-d24	576	37	51	Stiffened T-stub and bolt both yielded
TSS7-NP-d24	588	41	39	Stiffened T-stub and bolt both yielded

3.2. Distribution of the yield line

The parameters of the T-stubs affected not only the failure mode but also the yield line pattern of the connection. When the stiffened T-stub thickness increased from 8 mm to 12 mm, the failure mode of the connections varied from stiffened T-stub fracture to bolt fracture. By observing the final failure mode of the stiffened T-stubs with different thicknesses as shown in Figs. 3-5, it can be seen that the yield line patterns were also different. For the connection with the thickness of 8mm, the yield lines were distributed along the fracture position and bolt holes of the stiffened T-stub, as shown in Fig. 6(a). For the connection with the thickness of 10mm, the failure mode was the yield of both stiffened T-stub and bolt. The yield line pattern of the connection was closely related to the deformation of the stiffened T-stub, as shown in Fig. 6(b). As the thickness increased to 12mm, the failure mode was bolt failure with yielded stiffened T-stub. The yield line distribution of the connection was the same as that of the connection with the thickness of 10mm

When the horizontal bolt pitch g_H increased from 50mm to 90mm, the change in the length of the horizontal leg did not affect the failure mode of the connection. Therefore, the yield line distribution of the connection is shown in Fig. 6(b). The distance between the stiffener and bolt holes increased with the increase of longitudinal bolt pitch g_L. The greater the distance between the stiffener and the bolt hole was, the smaller the contact area ratio between the bolt and the stiffened T-stub became, which could affect the stiffness ratio between the bolt and the stiffened T-stub. Therefore, when g_L increased from 40mm to 60mm, the distribution of the yield line distribution of the connection varied from Fig. 6(b) to Fig. 6(a).

With the increase of bolt diameter d, the geometry of the stiffened T-stub did not change, indicating that the increase in diameter did not affect the failure mode of the connection. Therefore, the yield line mode of the connection did not change.

<table>
<tr><td>(a) Pattern 1</td><td>(b) Pattern 2</td></tr>
</table>

Fig. 6 Yield line distribution of the stiffened T-stub

Note: Q is prying force; B represents bolt force; B_y is the tensile yield capacity of the bolt; F is the tensile load.
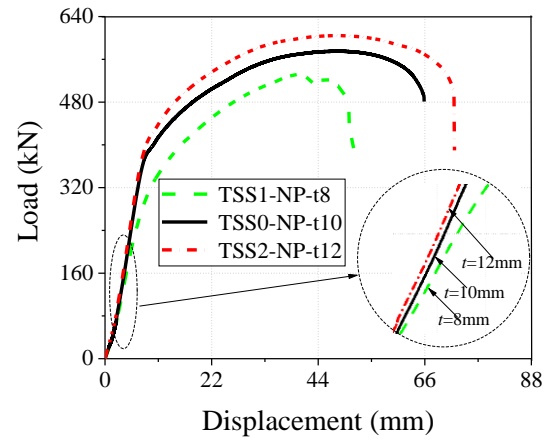
3.3. Load-displacement curves

151   Stiffened T-stub thickness t, horizontal bolt pitch g_H, longitudinal bolt pitch g_L, bolt diameter d and bolt

152 pretension P were the design parameters considered in this test. The effect of these parameters on connection

153 behavior will be discussed below by addressing the yield point, curve shape and failure mode of the specimens.

3.3.1 Stiffened T-stub thickness t

156   When the stiffened T-stub thickness t was 8mm, the fracture position appeared near the bolt hole line and

157 the weld seam. However, when the stiffened T-stub thickness was 10mm, the failure pattern was the yield of

158 both stiffened T-stub and bolt. When t increases from 8mm to 10mm, the yield strength and plastic

159 deformation of the connection both increase accordingly, as shown in Fig. 7 (a and b). When the stiffened

160 T-stub thickness is 12mm, the fracture pattern of TSS2-P-t12 was bolt fracture with yielded stiffened T-stub,

161 while the failure pattern of TSS2-NP-t12 was the yield of both stiffened T-stub and bolt. Therefore, it can be

162 concluded that bolt fracture causes the sudden drop in the load-displacement curve of TSS2-P-t12. Regarding

163 curve shape, all the curves present obvious three-stage characteristics, which indicate that the change of t does

164 not affect the shape of the curves.
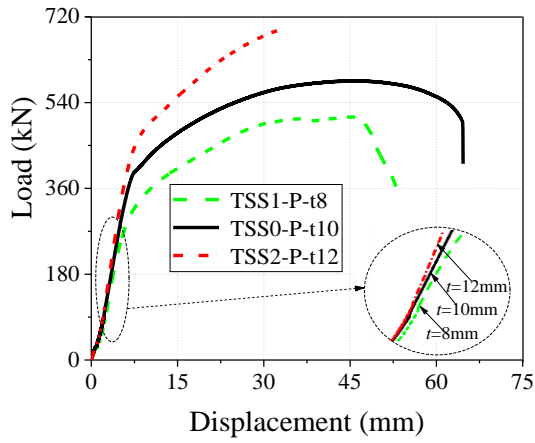
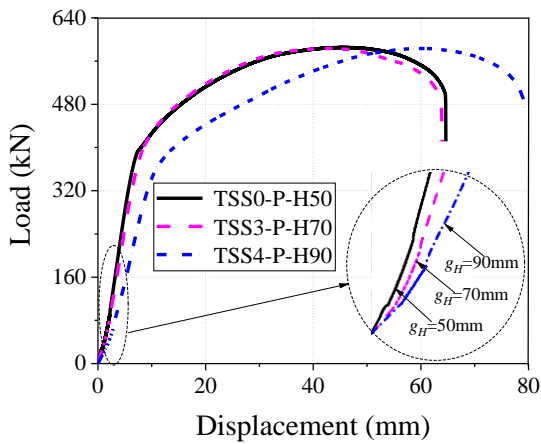(a) Load - displacement curve of the specimens

pre-tensioned

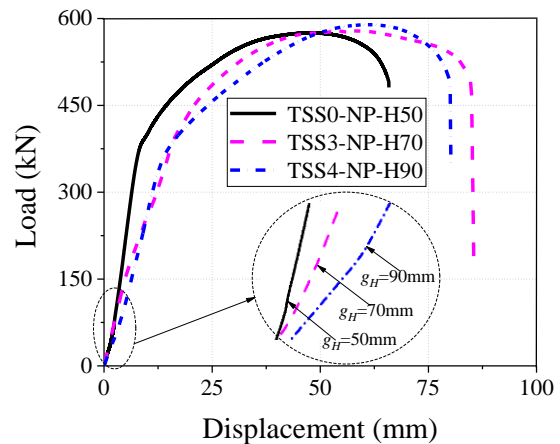(b) Load - displacement curve of the specimens not

pre-tensioned

Fig. 7 Effects of stiffened T-stub thickness (t)

3.3.2 Horizontal bolt pitch g_H

The change of horizontal bolt pitch g_H does not cause the change in the failure patterns of the connections, which were the yield of both stiffened T-stub and bolt. From the load-displacement curves as shown in Fig. 8, the stiffness of the connection decreases with the increase of g_H in the elastic stage of the curve. The yield point of the connection with bolt pretension decreases slightly with the increase of g_H, as shown in Fig. 8(a). When the curve enters the plastic deformation stage, the deformation stiffness and ultimate strength of the connection are not affected by the change of g_H.

(a) Load - displacement curve of the specimens

pre-tensioned

(b) Load - displacement curve of the specimens not

pre-tensioned

Fig. 8 Effects of horizontal bolt pitch (g_H)

11

3.3.3 Longitudinal bolt pitch g_L

As longitudinal bolt pitch g_L increases from 40mm to 60mm, the failure mode of stiffened T-stub changed from "completely yield" to "fracture near bolt hole line and weld seam", except for specimen TSS5-NP-L50. As shown in Fig. 9(b), the abrupt decline in the load-displacement curve of TSS5-NP-L50 during the plastic deformation stage is closely related to the failure pattern of the specimen, which was bolt fracture with yielded stiffened T-stub.

As shown in the load-displacement curves, the effect of g_L on connection performance is non-monotonic. From the shape of the curve, when g_L is 40mm and 50mm, the load-displacement curve of the connection is significantly different from that when g_L is 60mm. To find out the influence of g_L on connection performance, further parameter analysis would be carried out by using the finite element model in Section 4.
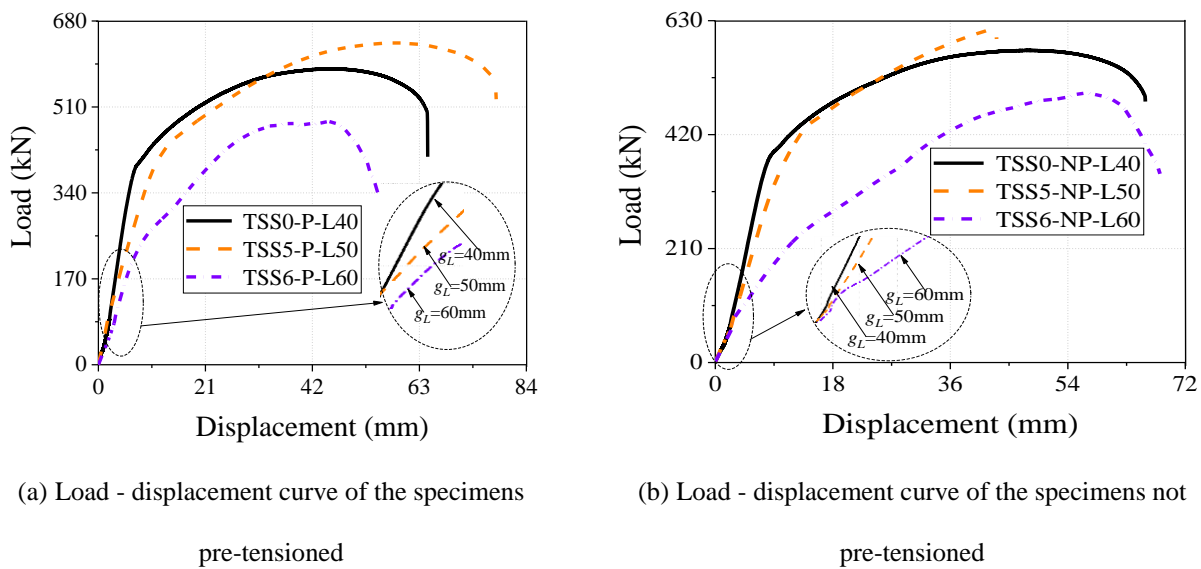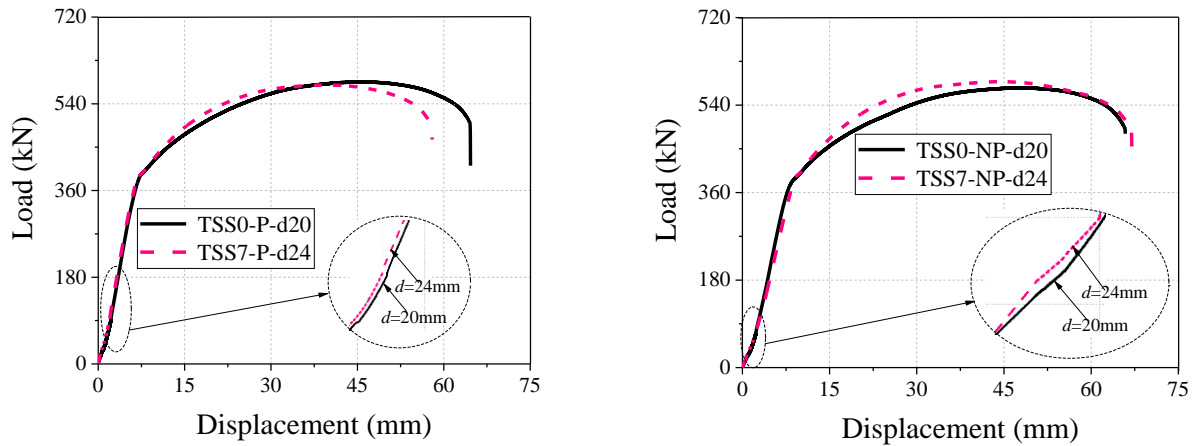

(a) Load - displacement curve of the specimens pre-tensioned

(b) Load - displacement curve of the specimens not pre-tensioned

Fig. 9 Effects of longitudinal bolt pitch (g_L)

3.3.4 Bolt diameter d

As the bolt diameter increases from 20mm to 24mm, the failure mode of stiffened T-stub was consistent. From the load-displacement curve, the yield points of the connections basically coincide, and the deformation stiffness of the specimens slightly increases. The shape of the curves is highly consistent, reflecting the obvious characteristics of three stages, as shown in Fig. 10. The influence of bolt diameter on the connection performance is not obvious, which would be further analyzed by changing the bolt diameter in the finite element models in Section 4.

(a) Load - displacement curve the specimens pre-tensioned   (b) Load - displacement curve of the specimens not

pre-tensioned

Fig. 10 Effects of bolt diameter (d)

3.3.5 Bolt pretension

As shown in Fig. 11, the initial stiffness of the connections increases when the pretension was applied to the

bolts. For the specimens with the same size, the shape of the curve is not affected by bolt pretension whilst the

yield strength of the connection is slightly increased by applying bolt pretension. With a few exceptions, such

as the group of TSS2 and TSS5, the failure mode of the specimens was not affected by bolt pretension.
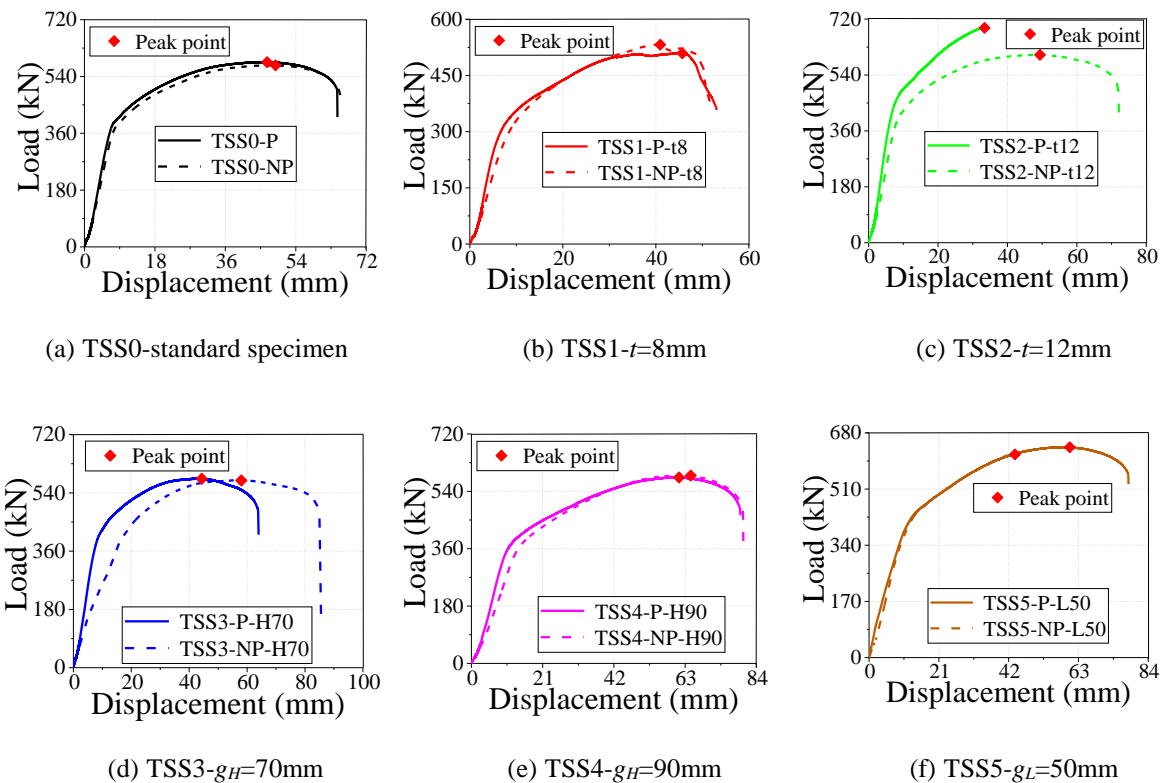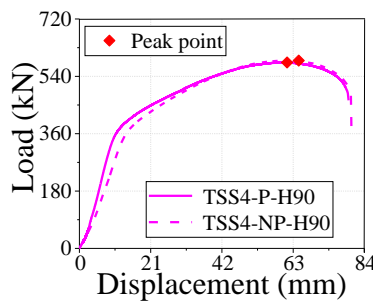

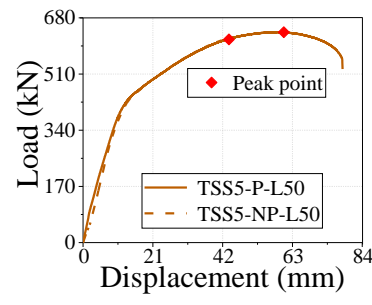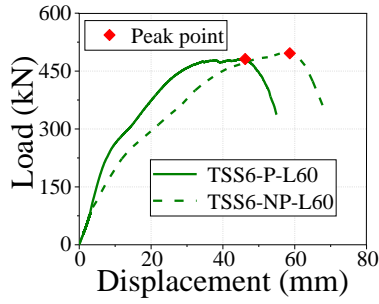(a) TSS0-standard specimen   (b) TSS1-t=8mm   (c) TSS2-t=12mm
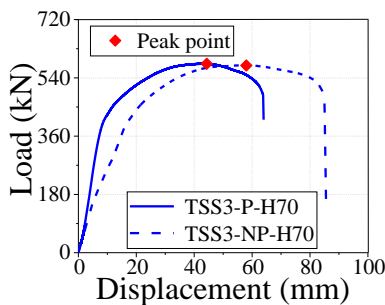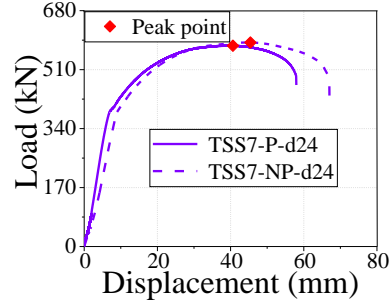
(d) TSS3-g_H=70mm   (e) TSS4-g_H=90mm   (f) TSS5-g_L=50mm

13

(g) TSS6-g_L=60mm　　　　　　　　　　　(h) TSS7-d=24mm

Fig. 11 Effects of bolt pretension (P)

4. Numerical simulation of bolted stiffened T-stub connection

4.1. Modeling techniques

To simulate the components in bolted stiffened T-stub connection, solid element (C3D8R) from ABAQUS library [34] is used to establish the finite element (FE) model. The dimension and material properties of the finite element model are consistent with those of the test specimens, as shown in Fig. 12. MERGE command is used to splice the T-stub and stiffeners into a whole. Since no crack in the weld seam was observed in the whole test process, welding seams are not simulated in the models.
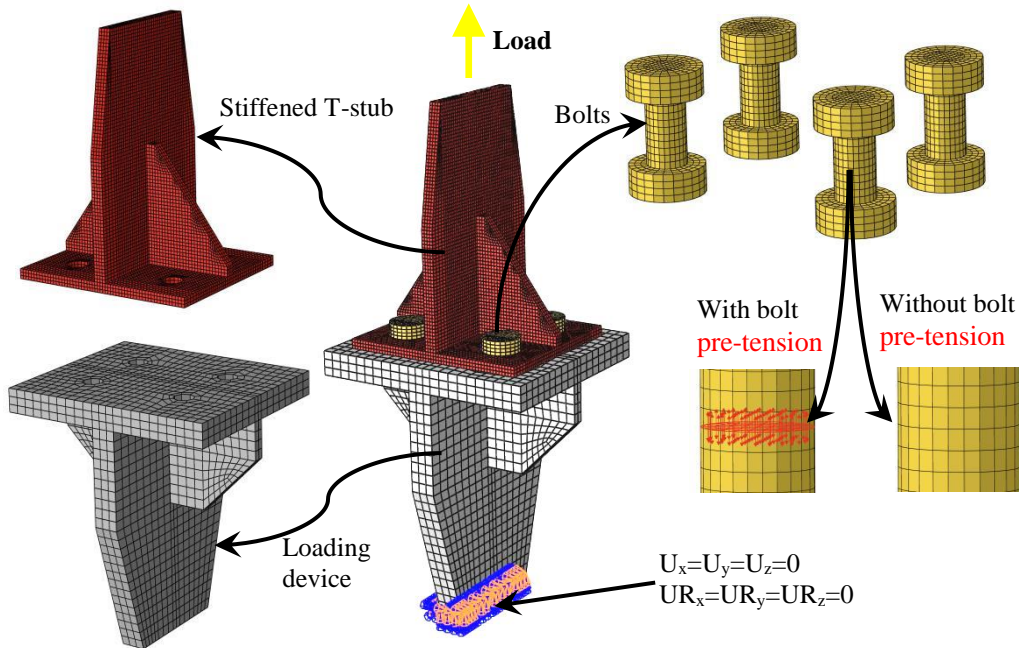

Fig. 12 FE model of the bolted stiffened T-stub connection

In the connection model, the contact between the components mainly exists in four places, including the pair of stiffened T-stub and loading device, screw and bolt hole, nut and stiffened T-stub, and screw head and

loading device. Since each component is a solid unit, the contact type is set as "Face to face contact". "Hard contact" in ABAQUS meaning that the contact pressure can be transferred between contact surfaces is used to present the normal contact in the model. The tangential contact is set as "Penalty" with a friction coefficient of 0.3.

4.2. Validation of finite element models

Fig. 13 compares the test and simulation results of the connections with bolt pretension. Regarding the shape of the curve, the simulation results are basically consistent with the experimental results. The peak points of the curves are marked in the figures. The ultimate strength of the simulation results is slightly higher than that of the experimental results, which is in a reasonable range. It can be seen that the simulation results are in good agreement with the test results when the bolt pretension is applied.

(a) TSS0-P (b) TSS1-P-t8 (c) TSS2-P-t12

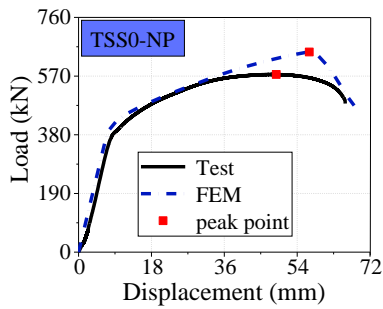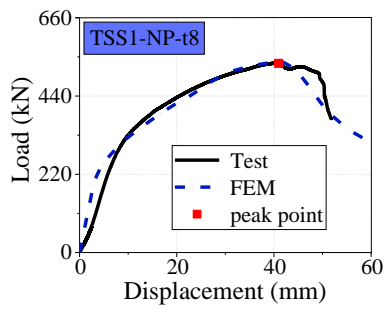(d) TSS3-P-H70 (e) TSS4-P-H90 (f) TSS5-P-L50
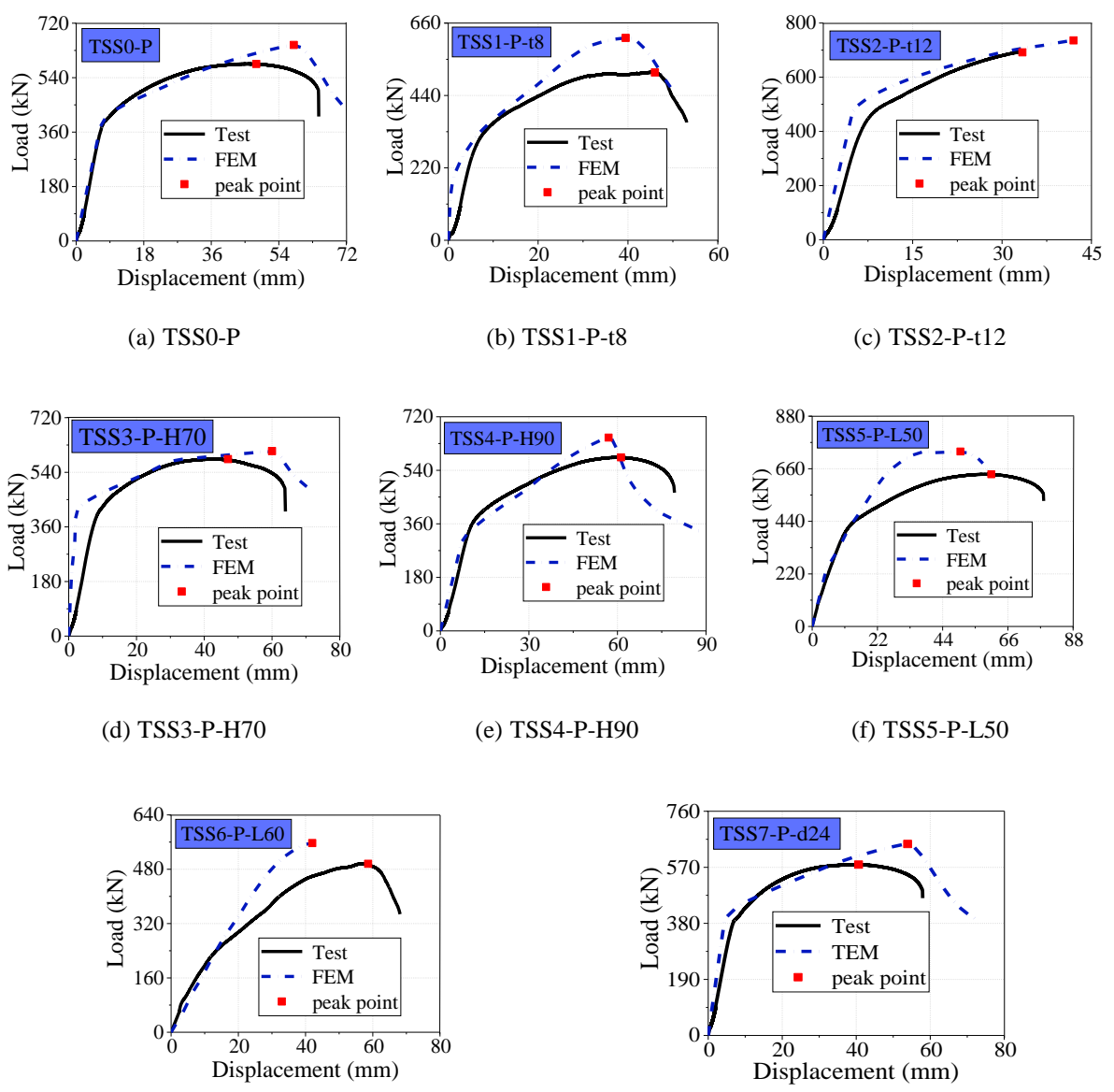
(g) TSS6-P-L60 (h) TSS7-P-d24

15

Fig. 13 Comparison of results between test and simulation (P)

For the specimens without bolt pretension, the nut was only tightened manually to keep the bolt from loosening during the test. Therefore, the bolts without pretension only play the role of connecting. Fig. 14 compares the simulation results and test results of the specimens without bolt pretension. There is little difference between the simulation results and the test results regarding the ultimate load and the initial stiffness of the connection. The curve features of the simulation results and test results show high similarity. It is also concluded that the existence of bolt pretension is beneficial to the simulation accuracy.
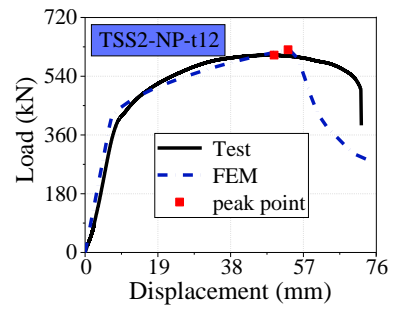
(a) TSS0-NP   (b) TSS1-NP-t8   (c) TSS2-NP-t12

(d) TSS3-NP-H70   (e) TSS4-NP-H90   (f) TSS5-NP-L50

(g) TSS6-NP-L60   (h) TSS7-NP-d24

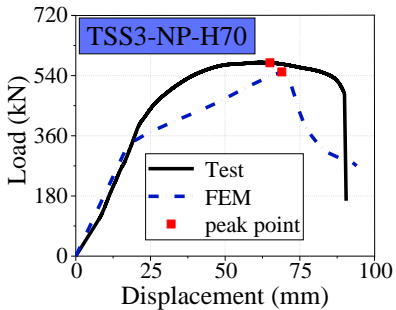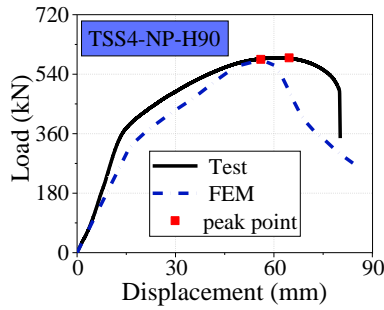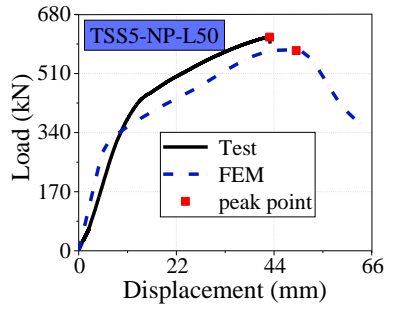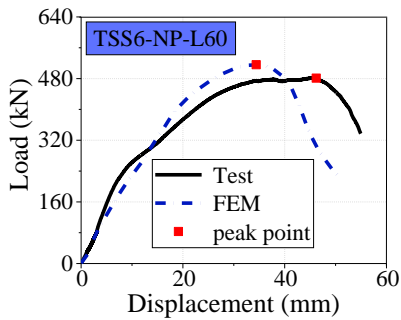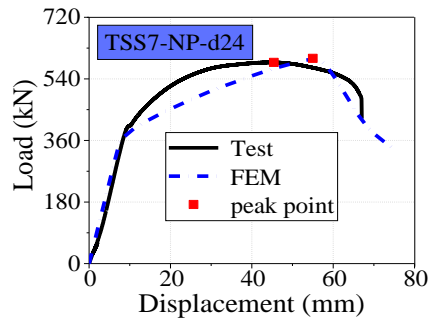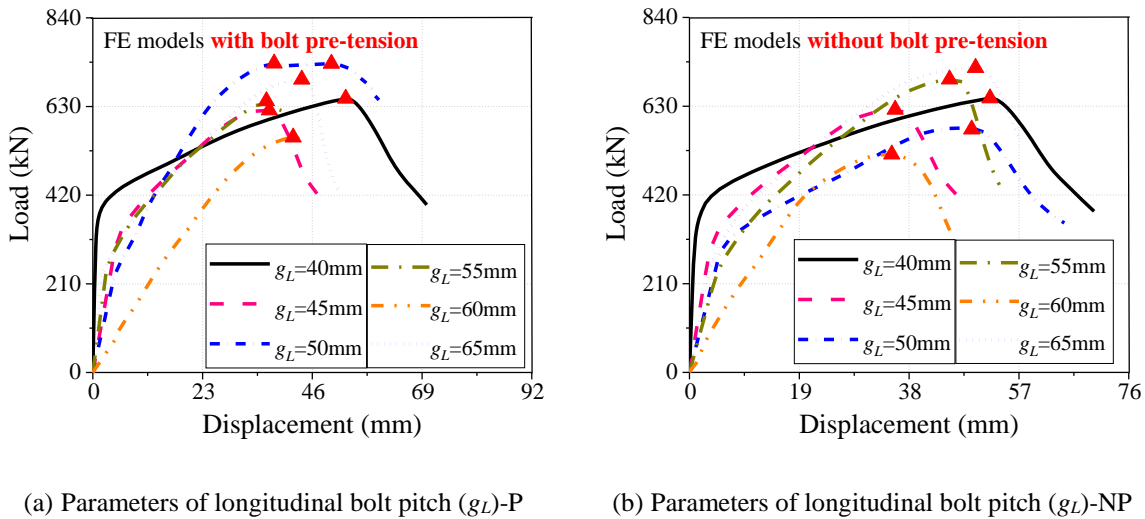Fig. 14 Comparison of results between test and simulation (NP)

219　It also should be admitted that the discrepancy between the experimental and simulation curves still exists.

220　Two reasons for the inaccuracy of the models are found: first, the contact between the components of the finite

221　element model is ideal. Test specimens need to be manually assembled, which leads to the contact between

222　components not being perfectly contacted. Second, clamp slip may occur at the early stage of loading, resulting

223　in a stiffness decline at the beginning of the load-displacement curve of the test.

4.3.　Parameters analysis

4.3.1 Longitudinal bolt pitch

226　The FE models with the longitudinal bolt pitch g_L of 40mm, 45mm, 50mm, 55mm, 60mm and 65mm are

227　developed. Fig. 15 shows the load-displacement curves of the models. It is worth mentioning that the change in

228　the ultimate strength and initial stiffness of the models are non-monotonic. Both the experimental results and

229　the simulation results show a similar variation law in the load-displacement relationship. It can be concluded

230　that the mechanical properties of the bolted stiffened T-stub connection are not monotonically related to the

231　change of g_L.

(a) Parameters of longitudinal bolt pitch (g_L)-P　　　(b) Parameters of longitudinal bolt pitch (g_L)-NP

Fig. 15 Comparison of results between test and simulation (g_L)

4.3.2 Bolt diameter

233　The models with bolt diameters of 14mm, 16mm, 18mm, 20mm and 24mm are analyzed. As shown in Fig.

234　16, the bolt diameter increases from 14mm to 20mm, the ultimate load of the models increases gradually.

235　When the bolt diameter increases from 20mm to 24mm, the ultimate deformation and ultimate strength of the

236　connection show little change. In general, the shape and characteristics of the curve are roughly the same,

237　including the stiffness of the plastic deformation stage.

17

(a) Parameters of bolt diameter (*d*)-P   (b) Parameters of bolt diameter (*d*)-NP
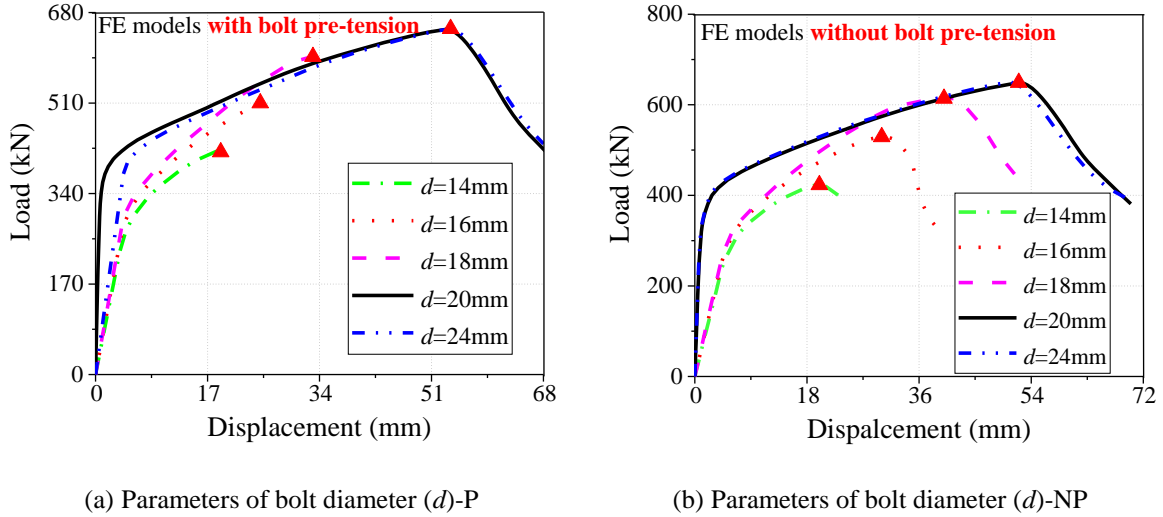
Fig. 16 Comparison of results between test and simulation (*d*)

4.3.3 Vertical plate thickness

To investigate the influence of vertical plate thickness t_V on the connection performance, four kinds of stiffened T-stub connection models with t_V=8mm/t=10mm, t_V=10mm/t=10mm, t_V=12mm/t=10mm and t_V=12mm/t=8mm are simulated in ABAQUS. As shown in Fig. 17, the load-displacement curves of the connections with equal thickness are compared with those of the connections with different thicknesses. When the thickness ratio of the vertical plate and horizontal plate is 6/5 (t_V=12mm/t=10mm), the ultimate strength of the connection is increased by 14%, compared with that of the connection under t_V=10mm/t=10mm. When the thickness ratio is 4/5 (t_V=8mm/t=10mm), the ultimate strength of the connection is reduced by 25%. When t_V is constant and t decreases from 10mm to 8mm, the ultimate strength and initial stiffness of the connection are reduced by 10%. Changing the thickness ratio of the vertical plate and horizontal plate has no significant effect on the ultimate deformation of the connection, but decreases the initial stiffness of the connection to a certain extent. It can be seen that, for conventional stiffened T-stub of equal thickness, properly increasing the thickness ratio of the vertical plate and horizontal plate can improve the ultimate strength of the connection.
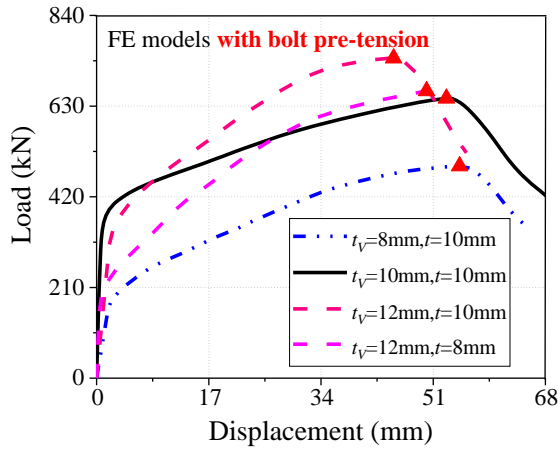
(a) Parameters of vertical plate thickness (t_V)-P   (b) Parameters of vertical plate thickness (t_V)-NP
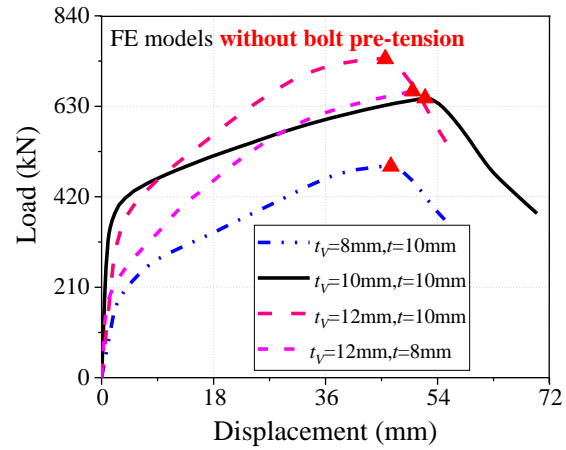
Fig. 17 Comparison of results between test and simulation (t_V)

5. Theoretical analysis of the bolted stiffened T-stub connection

Using the component method in EC3, T-stub is treated as the basic component in bolted connections. The performance of T-stub will directly affect the strength, stiffness and stability of beam-column joint, whose mechanical properties play a key role in the resistance to the progressive collapse of structures. In addition, a mechanical constitutive model of T-stub presented by the simplified spring element in EC3 can be used in the finite element simulation by using the spring truss model to further simplify the anti-collapse analysis of joints and structures.

However, EC3 does not directly provide the theoretical calculation method of stiffened T-stub connection. Therefore, a calculating method for the ultimate strength and initial stiffness of bolted stiffened T-stub connection is proposed in this study. First, the idea of the component method is adopted to split the connected components. Then, the strength and stiffness of each component are analyzed respectively. When the bolt pretension is applied, the bolt and the surrounding plate form a whole to jointly bear the external load. Without applying bolt pretension, only the bolts bear the tensile load. Therefore, the bearing capacity and stiffness of bolts with or without pretension are analyzed respectively. Finally, a prediction method for the ultimate strength and initial stiffness of stiffened T-stub connection is proposed based on test results and regression analysis.

5.1. Ultimate strength

5.1.1 Stiffener

The stiffened T-stub is divided into two parts: stiffener and T-stub. The equivalent truss model of stiffener [35] is shown in Fig. 18. The equivalent area A_e is

$$A_e = \eta \cdot h_e \cdot t_s \tag{2}$$

where η is a correction factor of equivalent area, $\eta=1.5$; t_s is the thickness of stiffener; h_e is the perpendicular to the hypotenuse of the triangle, as shown in Fig. 18 (b).

$$h_e = \frac{ab - c^2}{\sqrt{(a-c)^2 + (b-c)^2}} \tag{3}$$

where a, b and c can determine the shape and size of the stiffeners, as shown in Fig. 18.

(a) Stiffener in connection   (b) Geometry of stiffener [36]
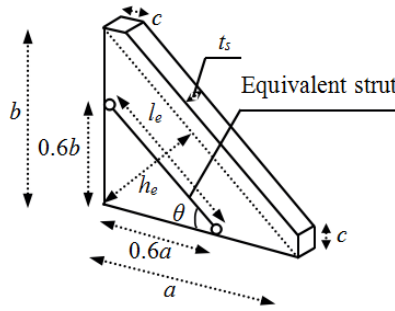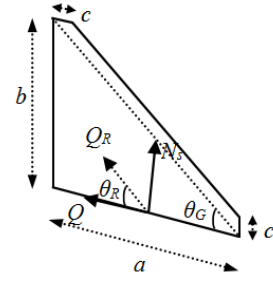
(c) forces developing at the

connection to stiffener interface [37]

Fig. 18 Stiffener in bolted stiffened T-stub connection

In the experiment, since the length of a and b of the stiffener is identical, the slope θ of the stiffener is 45°, which is slightly different from the assumption for the slope of the stiffener in Refs. [36,37].

The force at the connection interface of the stiffener is shown in Fig. 18(c).

$$N_s = \left(\frac{b}{a}\right) \cdot Q \tag{4}$$

According to Ref. [38], Q is calculated by the following formula:

$$Q = \frac{\dfrac{ad_b \cdot (0.21a + 0.51L')}{I_b}}{\dfrac{1}{\eta} \cdot \dfrac{0.6\sqrt{a^2 + b^2}\sqrt{(a-c)^2 + (b-c)^2}}{(ab - c^2)t} + \dfrac{(0.81b + 0.13d_b)(ad_b)}{I_b} \cdot V_{b,Ed}} \tag{5}$$

where d_b is the length of stiffened T-stub; I_b is the second moment of the area; $V_{B,Ed}$ is the design shear.

$$V_{B,Ed} = V_{B,Ed,M} + V_{B,Ed,G} \tag{6}$$

where $V_{B,Ed,M}$ is the shear force generated by plastic hinge formation of stiffened T-stub.

$$V_{B,Ed,M} = \frac{2 \cdot M_{B,Rd}}{L_h} \tag{7}$$

$V_{B,Ed,G}$ is caused by the gravity loads; L_h is the approximate distance between plastic hinges.

5.1.2 T-stub and bolt

The distribution of the yield line is related to the boundary condition and bolt hole distribution. The yield line distribution of T-stub is slightly different from that of stiffened T-stub. The ultimate tensile test of T-stub connection shows that the yield of T-stub diffused along the heel and bolt hole line. Therefore, the yield line is distributed along the heel and bolt hole line, as shown in Fig. 19. According to the yield line and the principle of limit equilibrium, the ultimate strength of T-stub is obtained:

$$N_{ut} = \frac{L_H t^2 f_u}{8 g_L} + \frac{(g_H + g_L) t^2 f_u}{2 g_H} \tag{8}$$

where L_H is the T-stub width.
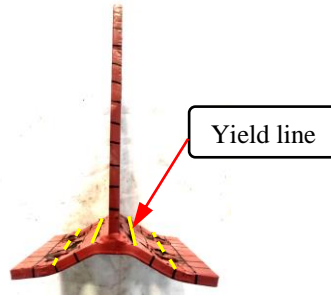
Fig. 19 Yielding line pattern of T-stub

When the bolt is not under pretension, the yield load of the bolt is taken as the ultimate strength of the bolt:

$$N_{u-NP}^b = f_{u,b} A_e \tag{9}$$

where $f_{u,b}$ is the bolt ultimate strength; $A_e = \pi(\frac{d_b}{2})^2$, d_b is the effective diameter of the bolt.

It is pointed out in Ref. [39] that when the pretension is applied to the bolt, the nut and its surrounding plate form a whole and share the tensile load. Therefore, the ultimate strength of the bolt after applying the pretension is

$$N_{u-P}^b = f_{u,b} \pi(\frac{d_b}{2})^2 + f_u \pi(\frac{1.2e - d_b}{2})^2 \tag{10}$$

where e is the maximum diameter of the nut, $e=40$ for M20 bolt and $e=44$ for M24 bolt.

5.1.3 Bearing integration

According to the test results and finite element analysis, the distribution of bolt holes and the size of T-stubs affect the overall performance of the connection. The bolt hole distribution on connection is affected by the parameters of horizontal bolt pitch g_H and longitudinal bolt pitch g_L. The main deformation of the T-shaped part is from the horizontal plate, therefore, the size of the T-shaped part is reflected in the length of the horizontal leg L_H and the length of the T-stub L_L. TSS-A0 is taken as the standard specimen (g_H=50mm, g_L=50mm, L_H=190mm, L_L=160mm), and the rest specimens are compared with TSS-A0. To better analyze the influence of parameter changes on the strength of the connection, the influence coefficients $(g_L/g_H)\times(L_H/L_L)$ of bolt hole distribution and T-stub size are given based on a series of regression analyses.

Due to bolt pretension, the bolt and the surrounding plate would translate together in the same direction. The bolt without pretension is an independent unit in load transfer. At this time, the actual distance between the stiffener and the bolt hole should be considered, which is $g_L-d/2$. Therefore, the strength of the stiffener on the whole connection without bolt pretension needs to be multiplied by the reduction factor, which is $(g_L-d/2)/g_L$.

Therefore, the calculation method of ultimate strength of bolted stiffened T-stub connection is

$$N_{u-P} = 4N_{ut} + (\frac{g_L}{g_H}\frac{L_H}{L_L}N_{u-P}^b + 2N_s) \quad \text{for pre-tensioned} \tag{11}$$

$$N_{u-NP} = 4N_{ut} + (\frac{g_L}{g_H}\frac{L_H}{L_L}N_{u-NP}^b + 2\frac{g_L-d/2}{g_L}N_s) \text{ for not pre-tensioned} \tag{12}$$

The prediction results of Eqs. (11-12) are compared with the test results and the ultimate strength calculation method based on cruciform stub model proposed by Xu et al. [40], as shown in Table 4. The predicted values by Eqs. (11-12) are in good agreement with the experimental results, and the error range is in the range of 0-10% approximately. The calculation method based on cruciform stub model provides a prediction which is 14-25% lower than the test value.

Table 4 Comparison of the predicted and tested ultimate strength

Specimen No.	Test [kN]	Eq. (11-12)		Eq. (11-12) error (%)	cruciform stub [40] [kN]	Error (%)
		N_{u-P} [kN] Eq.(10)	N_{u-NP} [kN] Eq.(11)			

TSS0-P	585	570	-	2.6	486	-16.9
TSS0-NP	575	-	547	4.9	486	-15.5
TSS1-P-t8	506	546	-	-7.9	435	-14.0
TSS1-NP-t8	532	-	517	2.8	435	-18.2
TSS2-P-t12	692	694	-	0.3	564	-18.5
TSS2-NP-t12	605	-	644	6.4	518	-14.4
TSS3-P-H70	584	573	-	1.9	486	-16.8
TSS3-NP-H70	578	-	523	9.5	486	-15.9
TSS4-P-H90	584	560	-	4.1	486	-16.8
TSS4-NP-H90	589	-	545	7.5	486	-17.5
TSS5-P-L50	579	608	-	-5.0	564	-2.6
TSS5-NP-L50	588	-	576	2.0	486	-17.3
TSS6-P-L60	585	617	-	-5.5	435	-25.6
TSS6-NP-L60	575	-	558	-3.0	435	-24.3
TSS7-P-d24	576	619	-	-7.4	486	-15.6
TSS7-NP-d24	588	-	596	-1.4	486	-17.3

5.2. Initial stiffness

Firstly, the stiffness of T-stub in bending and bolt in tension can be analyzed separately. Then, by considering the influence of different design parameters, the initial stiffness prediction formula of T-stub connection can be obtained by integrating the stiffness of T-stub in bending and bolt in tension. Finally, the relationship between T-stub and stiffened T-stub can be analyzed, which could be expressed in the form of coefficients. Consequently, the initial stiffness prediction method of stiffened T-stub connection can be obtained.

5.2.1 T-stub in bending

When the axial tension is smaller than the sum of the tensile strength of bolts and the friction force, it is believed that the rotation of the T-stub at the bolt hole line is rather small, approximately zero. Therefore, at the initial stage of loading, when the external load is less than the friction force, it is considered that the T-stub does not rotate. T-stub is symmetrical about the vertical plate, and the right part of the symmetrical plane is taken for analysis, as shown in Fig. 20. For calculation convenience, the bearing area of the T-stub is divided

340
1
2341
3
4
5
6
7
8
9
10
11
12
13
14
15
16
17
18
19
20
21
22342
23
24343
25
26344
27
28345
29
30
31346
32
33347
34
35348
36
37349
38
39
40350
41
42
43351
44
45
46352
47
48
49353
50
51
52354
53
54355
55
56
57356
58
59
60
61
62
63
64
65

into Plate I and Plate II along the centerline of the bolt hole to calculate the stiffness of the two regions
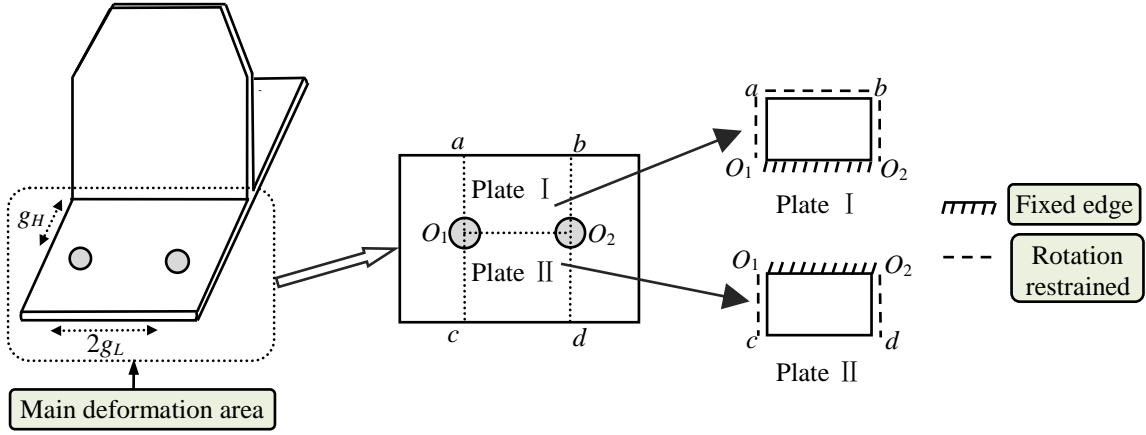
respectively.

Fig. 20 Simplified model of stiffened T-stub

Fig. 20 shows the simplified analytical model of the main deformation area of the T-stub. The horizontal

plates are divided into two segments, Plate I and Plate II along the centerline of the two bolt holes. The

distribution ratio is consistent with the test results. During the test, no deformation and failure occurred in the

loading device, indicating that the stiffness of the loading device was large enough to provide sufficient

constraints for the connection. Therefore, the loading device is regarded as a rigid body, and the stiffness of

the connection is only related to the bolts and T-stub.

According to the plate-shell theory, for a rectangular plate subjected to a concentrated load P, the

deflection at its central point is expressed by the following equation:

$$w_m = \frac{\alpha P a^2}{D} \tag{13}$$

where $D=Et^3/12(1-v^2)$; D is the flexural rigidity of the plate; v is the Poisson's ratio; E is the elastic modulus; t

is the plate thickness; a is the edge length; The literature [48] gives the value of α

$$\alpha_I = f(\lambda) = \begin{cases} 0.0084\lambda^{-0.732} & (\lambda \le 0.87) \\ 0.0093 & (\lambda > 0.87) \end{cases} \tag{14}$$

where $\lambda=b/a$; b is the side length of the fixed boundary.

Therefore, the deflection value at point a in Plate I can be obtained through Eqs. (13) and (14)

$$w_{Plate1} = \frac{P_a}{k_{epa}} \tag{15}$$

where k_{epa} is the stiffness at point a, $k_{epa} = \dfrac{D}{16\alpha_1 g_L^2} = \dfrac{Et^3}{48(1-v^2)F_I(g_H, g_L)}$; P_a is the acting force at point a; g_L

and g_H are shown in Fig. 20.

$$F_I(g_H, g_L) = \begin{cases} 0.336(2g_L)^2 \left(\dfrac{g_H}{2g_L}\right)^{-0.732} & \lambda \le 0.87 \\ 0.0372(2g_L)^2 & \lambda > 0.87 \end{cases} \tag{16}$$

The exact value of α for plate II is calculated by the following equation [41]:

$$\alpha_{II} = f(\lambda) = \frac{0.00725}{(1 + 4\lambda^{-7} + \lambda^{-14})^{1/7}} \tag{17}$$

Therefore, the deflection at point II on Plate c is:

$$w_{PlateII} = \frac{P_c}{k_{epc}} \tag{18}$$

$$k_{epc} = \frac{D}{16\alpha_{II} g_L^2} = \frac{Et^3}{48(1-v^2)F_{II}(g_H, g_L)} \tag{19}$$

$$F_{II}(g_H, g_L) = 4 f_{II}\left(\frac{g_H}{2g_L}\right)(2g_L)^2 = \frac{0.029 g_H^2 (2g_L)^2}{[g_H^{14} + (2g_L)^2 + 4g_H^7 (2g_L)^2]^{1/7}} \tag{20}$$

5.2.2 Bolt in tension

In Ref. [42,43], the following equation is used to calculate the stiffness of bolts without bolt pretension

$$k_{bt-NP} = 1.6 \frac{EA_b}{L_b} \tag{21}$$

where A_b and L_b are the effective area and length of bolt, according to EC3 [7]. When the bolt prying force is

taken into account, the coefficient is 1.6; otherwise, the value is 2.

After applying bolt pretension, the bolt and the plate around the bolt hole form an integral part. Therefore,

the bolt stiffness is controlled by the sum of the two [44,45].

$$k_{bp} = k_b + k_p \tag{22}$$

where k_p and k_b are plate stiffness around the bolt hole and the bolt stiffness, respectively. According to

reference [46], the relationship between k_p and k_b is:

$$\frac{k_p}{k_b} = 4.10 + 3.25 \frac{t_{ep} + t}{d_e} \tag{23}$$

The stiffness of pre-tensioned bolts from reference [39] is

25

$$k_{bt-P} = 2(5.10 + 3.25\frac{t_{ep}+t}{d_e})\frac{EA_b}{L_b} \tag{24}$$

where d_e is the effective diameter of bolt.

5.2.3 Stiffness integration

The stiffness of the bolt and T-stub is calculated respectively and then integrated to calculate the stiffness of the bolted stiffened T-stub connection.

If k_{I} and k_{II} are the stiffness of PlateI and PlateII, then

$$k_{\mathrm{I}} = \frac{P_{\mathrm{I}}}{w_{\mathrm{I}}} \; ; \; k_{\mathrm{II}} = \frac{P_{\mathrm{II}}}{w_{\mathrm{II}}} \tag{25}$$

where w_{I} and w_{II} are the final deformations of points a and c respectively.

$$k_{\mathrm{I}} = \frac{1}{\dfrac{1}{k_{ep\mathrm{I}}}+\dfrac{1}{k_{bt}}} \; , \; k_{\mathrm{II}} = \frac{1}{\dfrac{1}{k_{ep\mathrm{II}}}+\dfrac{1}{k_{bt}}} \tag{26}$$

$$k_{\mathrm{I}-P} = \frac{1}{\dfrac{1}{k_{ep\mathrm{I}}}+\dfrac{1}{k_{bt-P}}} \; ; \; k_{\mathrm{II}-P} = \frac{1}{\dfrac{1}{k_{ep\mathrm{II}}}+\dfrac{1}{k_{bt-P}}} \tag{27}$$

$$k_{\mathrm{I}-NP} = \frac{1}{\dfrac{1}{k_{ep\mathrm{I}}}+\dfrac{1}{k_{bt-NP}}} \; ; \; k_{\mathrm{II}-NP} = \frac{1}{\dfrac{1}{k_{ep\mathrm{II}}}+\dfrac{1}{k_{bt-NP}}} \tag{28}$$

Therefore, the calculation of the initial stiffness of bolted T-stub connections is shown in Eqs. (29) and (30)

$$k_{con-P} = 2[\frac{2g_L g_H}{(L_H-t_V)L_L}k_{\mathrm{I}-P} + \frac{(L_H-t_V-2g_H)/2}{L_H}k_{\mathrm{II}-P}] \quad \text{for pre-tensioned} \tag{29}$$

$$k_{con-NP} = 2[\frac{2g_L g_H}{(L_H-t_V)L_L}k_{\mathrm{I}-NP} + \frac{(L_H-t_V-2g_H)/2}{L_H}k_{\mathrm{II}-NP}] \quad \text{for not pre-tensioned} \tag{30}$$

Based on the force balance and deformation coordination conditions, the equations for the initial stiffness of the bolted stiffened T-stub connection are obtained as:

$$k_{con-NP}^s = k_{con-NP}/\mu \quad \text{for not pre-tensioned} \tag{31}$$

$$k_{con-P}^s = k_{con-P}/\mu \quad \text{for pre-tensioned} \tag{32}$$

where μ is the distribution coefficient of load, $\mu=A_T/(A_T+A_s)$, A_T is the area of the connecting surface between the rib stiffener and the vertical plate; A_S is the area of the connecting surface between the rib stiffener and the horizontal plate.

26

It can be seen from the derived results in Table 5 that the initial stiffness of the connection with bolt pretension is greater than that without bolt pretension. The influence of parameters t, g_H and g_L on the initial stiffness of the connection is consistent with that of the test value. The results predicted by Reinosa et al. [47] are also listed in Table 5. The error between the prediction from Eq. (31) or Eq. (32) and the tested values is within 0-10%, which is much smaller than the error between the prediction by Reinosa's formula and the tested results.

Table 5 Comparison of the predicted and tested initial stiffness					
Specimen No.	Test [kN/mm]	Eq. (31-32) [kN/mm]	Eq. (31-32) error (%)	Reinosa's formula [kN/mm]	Error (%)
TSS0-P	50	53	6.0	31	-38.0
TSS0-NP	38	37	-2.6	31	-18.4
TSS1-P-t8	39	36	-4.3	25	-35.9
TSS1-NP-t8	36	33	-8.3	25	-30.6
TSS2-P-t12	55	60	9.0	51	-7.3
TSS2-NP-t12	45	44	-2.2	51	13.3
TSS3-P-H70	42	44	4.7	23	-45.2
TSS3-NP-H70	18	19	5.6	23	27.8
TSS4-P-H90	33	30	-9.1	15	-54.5
TSS4-NP-H90	21	19	-9.5	15	-28.6
TSS5-P-L50	33	31	-6.1	31	-6.1
TSS5-NP-L50	31	33	6.5	31	0
TSS6-P-L60	28	26	-7.1	31	10.7
TSS6-NP-L60	18	19	5.6	31	72.2
TSS7-P-d24	51	55	7.8	31	-39.2
TSS7-NP-d24	39	37	5.1	31	-20.5

6. Conclusions

This paper studied the ultimate tensile behavior of the bolted stiffened T-stub connections. The failure modes, yield line distribution and mechanical properties of the connections were discussed in detail. Finite element models were used to verify and supplement the experimental results. The prediction methods for the

27

409   stiffness and tensile capacity of the bolted stiffened T-stub connection were deduced. The following

410   conclusions can be drawn:

411   1) Monotonic tensile tests were carried out on sixteen specimens by considering five different design

412   parameters: stiffened T-stub thickness t, horizontal bolt pitch g_H, longitudinal bolt pitch g_L, bolt diameter d and

413   bolt pretension. Three failure modes were observed, including the yield of both stiffened T-stub and bolt (TSS0,

414   TSS3, TSS4, TSS7, TSS2-NP-t12 and TSS5-P-L50), bolt fracture with yielded stiffened T-stub (TSS2-P-t12

415   and TSS5-NP-L50), stiffened T-stub fracture near bolt hole line and weld seam (TSS1 and TSS6).

416   2) The failure mode and yield line distribution of the stiffened connection changed with the change of the

417   stiffened T-stub thickness t and the longitudinal bolt pitch g_L. In addition, when t increased from 8mm to 12mm,

418   the ultimate strength of the connection was increased by 37% for the connections with pretension and 14% for

419   the connections without pretension. When g_L increased from 40mm to 60mm, the shape of the

420   load-displacement curve changed obviously, and the ultimate strength also increased first and then decreased.

421   The increase of horizontal bolt pitch g_H from 50mm to 90mm had the most significant effect on the initial

422   stiffness of the connection, which was decreased by 34% for the connections with pretension and 45% for the

423   connections without pretension.

424   3) The finite element models of bolted stiffened T-stub connections could well predict the key

425   characteristics of bolted stiffened T-stub connection including the stiffness, ductility, and ultimate strength of

426   the connection. Furthermore, the influence of bolt diameter, the longitudinal bolt pitch and the vertical plate

427   thickness of the stiffened T-stub on the connection performance was analyzed. The results of the parametric

428   analysis showed that increasing the thickness ratio of the vertical plate and horizontal plate could be helpful to

429   improve the ultimate strength of the connection.

430   4) The modified formulas for the ultimate strength of the stiffened connection with or without bolt

431   pretension were proposed respectively. The results from the proposed prediction method were compared with

432   the results from the test and cruciform stub method. The errors of the formulas presented in this paper were in

433   the range of 0-10%. The ultimate strength provided by the cruciform stub method was 14-25% lower than the

434   test value.

435   5) The modified formulas for the initial stiffness of the stiffened connection with or without bolt pretension

436   were proposed respectively. The results from the proposed prediction method were compared with the test

results and Reinosa's formula. The errors of the formulas presented in this paper were in the range of 0-10%, which is much smaller than the error between the prediction by Reinosa's formula and the tested results.

Acknowledgement

References

[1] United States General Services Administration (GSA). Progressive collapse analysis and design guidelines for new federal office buildings and major modernization projects. Washington (DC). 2003.

[2] Department of Defense (DoD). Unified facilities criteria (UFC): design of structures to resist progressive collapse. Washington (DC). 2009.

[3] B. Yang, K.H. Tan, Experimental tests of different types of bolted steel beam-column joints under a central-column-removal scenario, Eng. Struct. 54 (2013) 112-130.

[4] Q.N. Fu, B. Yang, Y. Hu, Dynamic analyses of bolted-angle steel joints against progressive collapse based on component-based model, J. Constr. Steel Res. 117 (2016) 161-174.

[5] Y.L. Gong, Test, modeling and design of bolted-angle connections subjected to column removal, J. Constr. Steel Res. 139 (2017) 315-326.

[6] M. Xu, S. Gao, B. Yang, Z. Peng, Study on seismic behavior of angle steel connection joints for concrete-filled square steel tubular column, Ing. Sismica. 35 (2018) 139-157.

[7] Eurocode 3, Design of steel structures. Part 1.8, design of joints, European Committee for Standardization, 2005.

[8] A. Loureiro, R. Gutiérrez, J.M. Reinosa, Axial stiffness prediction of non-preloaded T-stubs: Analytical frame approach, J. Constr. Steel Res. 66 (2010) 1516-1522.

[9] J.M. Reinosa, A. Loureiro, R. Gutierrez, M. Lopez, Analytical frame approach for the axial stiffness prediction of preloaded T-stubs, J. Constr. Steel Res. 90 (2013) 156-163.

[10] J.M. Reinosa, A. Loureiro, R. Gutierrez, M. Lopez, Analytical frame approach for the rotational stiffness prediction of beam-to-column angle connections, J. Constr. Steel Res. 106 (2015) 67-76.

[11] X.Z. Zhao, S.B. He, S.Yan, Full-range behavior of T-stubs with various yield line patterns, J. Constr. Steel Res. 186 (2021) 106919.

[12] J.P. Jaspart, R. Maquoi, Prediction of the semi-rigid and partial strength properties of structural joints, in: Proceedings of the SSRC Annual Technical Session and Meeting, Lehigh, 1994.

[13] V. Saberi, M. Gerami, A. Kheyroddin, Comparison of bolted end plate and T-stub connection sensitivity to component thickness, J. Constr. Steel Res. 98 (2014) 134-145.

[14] H. Tagawa, Y.D. Liu, Stiffening of bolted end-plate connections with steel member assemblies, J. Constr. Steel Res. 103 (2014) 190-199.

[15] Y. O. ¨Ozkılıç. The capacities of unstiffened T-stubs with thin plates and large bolts, J. Constr. Steel Res. 186 (2021) 106908.

[16] B. Gil, F. Bijlaard, E. Bayo, T-stub behavior under out-of-plane bending. II: Parametric study and analytical characterization, Eng. Struct. 98 (2015) 241-250.

[17] J. Shen, A. Astaneh-Asl, Hysteretic behavior of bolted-angle connections, J. Constr. Steel Res. 51 (1991) 201-218.

[18] J. Shen, A. Astaneh-Asl, Hysteresis model of bolted-angle connections, J. Constr. Steel Res. 54 (2000) 317-343.

[19] C. Malaga-Chuquitaype, A.Y. Elghazouli, Component-based mechanical models for blind-bolted-angle connections, Eng. Struct. 32 (2010) 3048-3067.

[20] J. Ribeiro, A. Santiago, C. Rigueiro, L.S. da Silva, Analytical model for the response of T-stub joint component under impact loading, J. Constr. Steel Res. 106 (2015) 23-34.

[21] L. Massimo, R. Gianvittorio, S. Aldina, S. da Silva Luis, Experimental analysis and mechanical modeling of T-stubs with four bolts per row, J. Constr. Steel Res. 101 (2014) 158-174.

[22] A.C. Faralli, M. Latour , P.J. Tan, G. Rizzano, P. Wrobel, Experimental investigation and modeling of T-stubs undergoing large displacements, J. Constr. Steel Res. 180 (2021) 106580.

[23] A.B. Francavilla, M. Latour, V. Piluso, G. Rizzano, Simplified finite element analysis of bolted T-stub connection components, Eng. Struct. 100 (2015) 656-664.

[24] O.S. Bursi, J.P. Jaspart, Benchmarks for Finite Element Modelling of Bolted Steel Connections, J. Constr. Steel Res. 43 (1997) 17-42.

[25] H.R. Sebbagh, D. El Ddine Kerdal, A. Abidelah, A. Bouchaïr, T-stubs with two and four bolts under monotonic and cyclic loading, J. Constr. Steel Res. 178 (2021) 106486.

[26] B. Yang, K.H. Tan, Robustness of bolted-angle connections against progressive collapse: mechanical modeling of bolted-angle connections under tension, Eng. Struct. 57 (2013) 153-168.

[27] Y.L. Gong, Ultimate tensile deformation and strength capacities of bolted-angle connections, J. Constr. Steel Res. 100 (2014) 50-59.

[28] R. Timmers, Generalized method for identifying yield-line patterns in T-stubs using discontinuity layout optimization, Eng. Struct. 244 (2021) 112802.

[29] L.M. Bezerra, J. Bonilla, W.A. Silva, W.T. Matias, Experimental and numerical studies of bolted T-stub steel connection with different flange thicknesses connected to a rigid base, Eng. Struct. 218 (2020) 110770.

[30] P. Barata, J. Ribeiro, C. Rigueiro, A. Santiago, J.P. Rodrigues, Assessment of the T-stub joint component at ambient and elevated temperatures, Fire Safety J. 70 (2014) 1-13.

[31] F. Gao, Z.X. Liu, X.Q. Guan, Fire resistance behavior of T-stub joint components under transient heat transfer conditions, Eng. Struct. 237 (2021) 112164.

[32] P.J. Wang, Y. You, Q.H. Wang, H.P. Gu, G.W. Wang, Y.J. Liu, F.Z. Liu, Post-fire tensile behavior of hole-anchored bolted T-stub connection, J. Constr. Steel Res. 187 (2021) 106941.

[33] I. Both, D. Duma, F. Dinu, D. Dubina, R. Zaharia, The influence of loading rate on the ultimate capacity of bolted T-stubs at ambient and high temperature, Fire Safety J. 125 (2021) 103438.

[34] W. Qi, ABAQUS 6.14 Super Learning Manual, People's posts and telecommunications publishing house, 2016.

[35] C.-H. Lee, Seismic design of rib-reinforced steel moment connections based on Equivalent Strut Model, J. Struct. Eng. ASCE. 128 (2002) 1121-1129.

[36] A. Abidelah, A. Bouchaïr, D.E. Kerdal, Experimental and analytical behavior of bolted end-plate connections with or without stiffeners, J. Constr. Steel Res. 76 (2012) 13-27.

[37] C.-H. Lee, J.-H. Jung, M.-H. Oh, E.-S. Koo, Experimental study of cyclic seismic behavior of steel moment connections reinforced with ribs, J. Struct. Eng. ASCE. 131 (2005) 108-118.

[38] M. D'Aniello, R. Tartaglia, S. Costanzo, R. Landolfo, Seismic design of extended stiffened end-plate joints in the framework of Eurocodes, J. Constr. Steel Res. 128 (2017) 512-527.

[39] Z.Q. Wu, Beam-to-column bolted extended endplate connection and its influence on frame behavior, PhD Thesis, Harbin Institute of Technology, 2008.